Comparative analysis between AVO and elastic inversion emphasizing the influence of low-frequency components in the characterization of seismic anomalies.

Glauco M. Sousa (UFBA and PETROBRAS), Carlos L. Varela (PETROBRAS), Paulo M. de Carvalho (PETROBRAS) and Amin Bassrei (UFBA)

Abstract

This paper presents a comparison between AVO and elastic inversion techniques emphasizing the influence of low-frequency components in the characterization of anomalies related to hydrocarbon. It is shown that in some situations a simple AVO analysis is more efficient to discriminate anomalies related to hydrocarbon mainly when well logs are sparse i.e., when empirical relationships are used to estimate the low-frequency components of v_s and ρ and also when there is a gap between the provided low-frequency (from wells and/or seismic velocities) and high-frequency (seismic amplitudes) components for the elastic inversion procedure. These techniques were applied in a synthetic seismogram generated from a hypothetical set of elastic logs.

Introduction

The large variety of source/receiver offsets considered in the acquisition of conventional surface seismic data, based on the CDP technique, provides a high multiplicity of information about the subsurface. The quasi hyperbolic two way reflection time curves in CDP gathers carry information about the low-frequency components of the velocity model, also known as the macro velocity model. On the other hand, the amplitude variations with offset (AVO) carry information about elastic property contrasts across the interfaces and are limited to the frequency band of the seismic signature. Regardless of all this information, during several years, seismic exploration in the petroleum industry was based on the reflection times on stacked seismic data. However, in the last few decades, techniques based on prestack data information, such as AVO and elastic inversion techniques, have been developed to help interpreters to identify and validate seismic anomalies. The AVO technique generally aims to qualitatively/statistically characterize the subsurface. This technique basically identifies anomalous seismic events that do not follow the expected behavior for brine saturated rocks, also known as the background trend. The anomalous events are generally associated with the presence of hydrocarbon saturated reservoirs or anomalous rocks in subsurface. On the other hand, elastic inversion aims to quantitatively/deterministically characterize the subsurface, estimating the absolute values of the elastic properties that characterize the investigated rocks. These differences fundamentally lie on different methodologies applied to deconvolution and also to the inclusion of low-frequency components in the elastic inversion procedure. In practical terms, in the AVO technique, the deconvolution is usually performed through the estimation of wavelet based on the seismic data themselves, while in elastic inversion one uses the information on the reflectivity extracted from the available wells for estimating the wavelet that produces a best fit between the observed and calculated amplitudes. The estimates of AVO parameters exclusively depend on seismic amplitudes, so that the estimated parameters have a band-limited nature, and anomaly characterization is done statistically by the deviation from the background trend. Besides the seismic amplitudes, the elastic inversion also uses well information and the reflection time curves in the CDP gathers. In this case, the anomaly definition is made quantitatively from cutoff values defined from well data.

Synthetic data

The Figure 1 shows a hypothetical set of elastic logs composed by compressional velocity, shear velocity and density. Utilizing a butterworth wavelet (Figure 2) and the elastic parameters from these logs, it was generated a synthetic CDP gather utilizing the convolutional model (Figure 3). Constant incidence angle traces or angle traces compose this CDP gather. The two negative amplitude events at 0.4 and 1.4 s correspond to the tops of a gas-saturated sandstone and an oil-saturated sandstone, respectively.
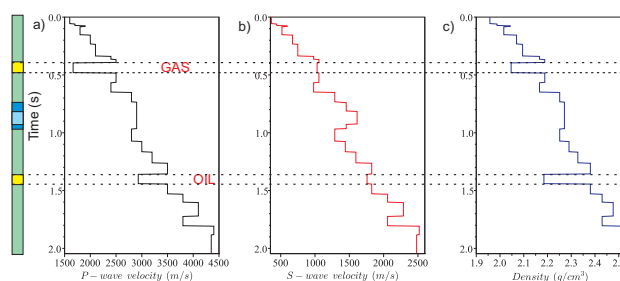

Figure 1: Hypothetical set of elastic logs: (a) Compressional velocity, (b) shear velocity and (c) density. The yellow color in lithologic column indicates the hydrocarbon-saturated sandstones.
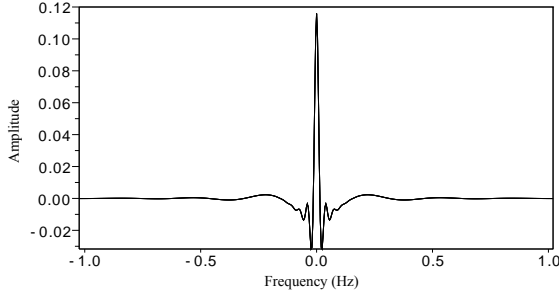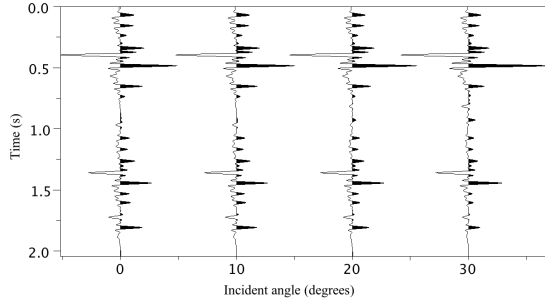
Figure 2: A zero-phase wavelet.

Figure 3: CDP gather composed by angle-traces.

Forward modeling

For the AVO analysis, we used the approximation for reflection coefficient as a function of incidence angle proposed by Aki and Richards (1980):

$$r(\theta) = A + B\sin^2\theta + C\sin^2\theta\tan^2\theta, \qquad (1)$$

where $r(\theta)$ is the reflection coefficient. The parameters A, B and C are given by:

$$A = \frac{1}{2}\left(\frac{\Delta v_p}{v_p} + \frac{\Delta\rho}{\rho}\right) = \frac{1}{2}\frac{\Delta I_P}{I_P}, \qquad (2)$$

$$B = -kA + (1-k)C + k\left(\frac{\Delta v_p}{v_p} - \frac{\Delta v_s}{v_s}\right), \qquad (3)$$

and

$$C = \frac{1}{2}\left(\frac{\Delta v_p}{v_p}\right), \qquad (4)$$

where v_p, v_s, ρ and I_P are the average of compressional velocity, shear velocity, density and acoustic impedance for the two media, respectively. The parameter k depends on the ratio between v_s and v_p, i.e:

$$k = 4(v_s/v_p)^2. \qquad (5)$$

Rewriting the equation 1 in matrix form:

$$\begin{bmatrix} r_1 \\ r_2 \\ \vdots \\ r_j \end{bmatrix} = \begin{bmatrix} 1 & \mathrm{sen}^2\theta_1 & \mathrm{sen}^2\theta_1\tan^2\theta_1 \\ 1 & \mathrm{sen}^2\theta_2 & \mathrm{sen}^2\theta_2\tan^2\theta_2 \\ \vdots & \vdots & \vdots \\ 1 & \mathrm{sen}^2\theta_j & \mathrm{sen}^2\theta_j\tan^2\theta_j \end{bmatrix} \underbrace{\begin{bmatrix} A \\ B \\ C \end{bmatrix}}_{\mathbf{m}}, \qquad (6)$$

$$\underbrace{}_{\mathbf{d}^{cal}} \qquad \underbrace{}_{G}$$

where $\mathbf{r}_j$ represents the jth reflection coefficient calculated in the jth incidence angle θ, G is an $j \times 3$ matrix and $\mathbf{m}$ is an 3×1 vector containing the models parameters A, B and C.

The methodology proposed for elastic inversion utilizes an equivalent approximation to describe the reflection coefficient variation as a function of the incident angle (Fatti et al., 1994):

$$r(\theta) = A(1 + \tan^2\theta) - D(2k\sin^2\theta) + E(k\sin^2\theta - \tan^2\theta) \quad (7)$$

where the parameters D and E are defined as:

$$D = \frac{1}{2}\frac{\Delta I_S}{I_S} \qquad (8)$$

and

$$E = \frac{1}{2}\frac{\Delta\rho}{\rho}, \qquad (9)$$

where I_S is the average of shear impedance for the two media. The term k is determined from the background trend, i.e by low-frequency components of v_s and v_p.

A seismic trace x can be obtained by the convolution between the reflection coefficient r and the wavelet w for a given incidence angle θ:

$$x(\theta) = r(\theta) * w(\theta). \qquad (10)$$

Substituting equation 7 into equation 10 and showing the result in matrix form for k angle-trace as done by Hampson and Russell (2005):

$$\underbrace{\begin{bmatrix} \mathbf{x}(\theta_1) \\ \mathbf{x}(\theta_2) \\ \vdots \\ \mathbf{x}(\theta_k) \end{bmatrix}}_{\mathbf{x}^{cal}} = \underbrace{\begin{bmatrix} c_1(\theta_1)w(\theta_1) & c_2w(\theta_1) & c_3w(\theta_1) \\ c_1(\theta_1)w(\theta_2) & c_2w(\theta_2) & c_3w(\theta_2) \\ \vdots & \vdots & \vdots \\ c_1(\theta_k)w(\theta_k) & c_2w(\theta_k) & c_3w(\theta_k) \end{bmatrix}}_{Q} \underbrace{\begin{bmatrix} A \\ D \\ E \end{bmatrix}}_{m}$$

$$(11)$$

where $\mathbf{x}^{cal}$ is an $N \times 1$ vector containing the angle-traces calculated, Q is an $N \times N$ matrix and $\mathbf{m}$ is an $N \times 1$ vector containing the model parameters $\mathbf{A}$, $\mathbf{D}$ and $\mathbf{E}$ for all time samples. The others coefficients are given by: $c_1(\theta) = 1 + \tan^2\theta$, $c_2(\theta) = -2k\mathrm{sen}^2\theta$ and $c_3(\theta) = k\mathrm{sen}^2\theta - \tan^2\theta$.

Objective function

Both AVO and elastic inversion utilize an objective function based on the premise that the sum of squared differences between observed and calculated seismic data would be the minimum.

For AVO analysis the objective function J_a is evaluated for each time sample:

$$J_a = (\mathbf{d} - \mathbf{d}^{cal})^T(\mathbf{d} - \mathbf{d}^{cal}), \qquad (12)$$

where $\mathbf{d}$ is the observed seismic data and $\mathbf{d}^{cal}$ is the calculated one utilizing by Aki and Richards (1980) approximation. Substituting equation 6 into equation 12 and then minimizing equation 12 in relation to A, B and C:

$$\mathbf{m}^{est} = (G^T G)^{-1} G^T \mathbf{d}, \qquad (13)$$

where $\mathbf{m}^{est} = [A,B,C]^T$ and the G matrix is indicated in equation 6.

Elastic inversion utilizes the objective function J_e similar to the previous one, but the misfit is evaluated for all time samples together. In order to recover absolute values from the seismic data and to reduce ambiguity it is necessary to include low-frequency components. These components were introduced as a prior information in the inversion process as elastic extension of the methodology proposed by Velis (2006). Considering the logarithmic approximation that allows the establishment of a relationship between reflectivities parameters and elastic parameters: (valid for $|A|$, $|D|$ and $|E|$ lower than < 0.3):

$$A_i = \frac{1}{2}\Delta\ln I_{P_i}, \tag{14}$$

$$D_i = \frac{1}{2}\Delta\ln I_{S_i} \tag{15}$$

and

$$E_i = \frac{1}{2}\Delta\ln\rho_i. \tag{16}$$

Then:

$$A_{I_i} = \sum_{j=1}^{i} A_j = \frac{1}{2}\ln\frac{I_{P_i}}{I_{P_0}}, \tag{17}$$

$$D_{I_i} = \sum_{j=1}^{i} D_j = \frac{1}{2}\ln\frac{I_{S_i}}{I_{S_0}}, \tag{18}$$

and

$$E_{I_i} = \sum_{j=1}^{i} E_j = \frac{1}{2}\ln\frac{\rho_i}{\rho_0}, \tag{19}$$

where I_{P_0}, I_{S_0} and ρ_0 are the acoustic impedance, shear impedance and density at surface, respectively. A_I, D_I and E_i are the acoustic impedance, shear impedance and density constraint at the layer i.

We can rewriting the equation 17 in the matrix form:

$$\underbrace{\begin{bmatrix} A_{I_1} \\ A_{I_2} \\ A_{I_3} \\ \vdots \\ A_{I_N} \end{bmatrix}}_{\mathbf{A_I}} = \underbrace{\begin{bmatrix} 1 & 0 & 0 & \ldots & 0 \\ 1 & 1 & 0 & \ldots & 0 \\ 1 & 1 & 1 & \ldots & 0 \\ \vdots & \vdots & \vdots & \vdots & \vdots \\ 1 & 1 & 1 & \ldots & 1 \end{bmatrix}}_{U} \underbrace{\begin{bmatrix} A_1 \\ A_2 \\ A_3 \\ \vdots \\ A_N \end{bmatrix}}_{\mathbf{A}}, \tag{20}$$

where U corresponds to an integration matrix. Extending the previous relationship for the others parameters involved:

$$\underbrace{\begin{bmatrix} \mathbf{A_I} \\ \mathbf{D_I} \\ \mathbf{E_I} \end{bmatrix}}_{\xi} = \underbrace{\begin{bmatrix} U & Z & Z \\ Z & U & Z \\ Z & Z & U \end{bmatrix}}_{C} \underbrace{\begin{bmatrix} \mathbf{A} \\ \mathbf{D} \\ \mathbf{E} \end{bmatrix}}_{\mathbf{m}}, \tag{21}$$

where Z is a zero matrix.

Now we can define the objective function for elastic inversion as:

$$J_e = (\mathbf{x}-\mathbf{x}^{cal})^T(\mathbf{x}-\mathbf{x}^{cal}) + (\xi-\xi^{cal})^T(\xi-\xi^{cal}) \tag{22}$$

where $\mathbf{x}$ and $\mathbf{x}^{cal}$ are the corresponding observed and calculated angle-traces. ξ and ξ^{cal} are the provided

and calculated low-frequency components. Minimizing the previous equation with respect to A, D and E:

$$\mathbf{m}^{est} = (F+\beta I)^{-1}(G^T\mathbf{x}+\varepsilon C^T\xi), \tag{23}$$

where $F = Q^T Q + \varepsilon C^T C$ and $\mathbf{m}^{est}$ is a vector containing $\mathbf{A}$, $\mathbf{D}$ and $\mathbf{E}$. I is the identity matrix, β is the damping constant and ε is the weight given for the a prior model.

The reflectivity parameters obtained in the solution given by equation 23 are inverted to estimate I_P, I_S and ρ using the following equations:

$$I_{P_i} = I_{P_0}\prod_{k=1}^{i}\frac{1+A_i}{1-A_i}. \tag{24}$$

$$I_{S_i} = I_{S_0}\prod_{k=1}^{i}\frac{1+D_i}{1-D_i}. \tag{25}$$

and

$$\rho_i = \rho_0\prod_{k=1}^{i}\frac{1+E_i}{1-E_i}. \tag{26}$$

AVO

The estimated AVO parameters were integrated to generate layer parameters to allow comparisons with parameters obtained from elastic inversion. The Figure 4 shows the true AVO parameters obtained from well logs (superscript true), the estimated parameters (superscript est) and the associated errors in the form of traces. It was observed that the parameters $\mathbf{A}^{est}$ and $\mathbf{B}^{est}$ were very well estimated. The parameter $\mathbf{C}^{est}$ presents the significant errors mainly in the intervals presenting large elastic contrasts.
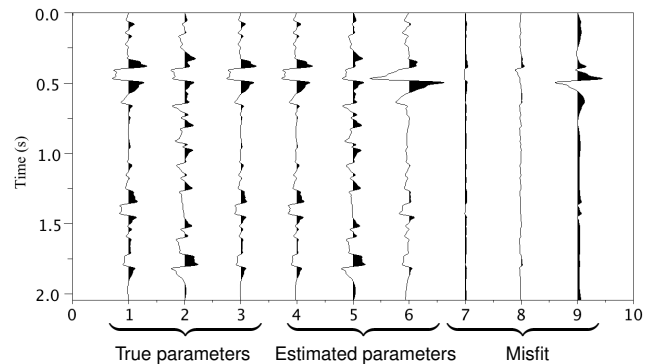

Figure 4: Quality control of the estimated AVO parameters. Traces 1 to 3: true parameters $\mathbf{A}^{true}$, $\mathbf{B}^{true}$, $\mathbf{C}^{true}$ generated from well logs; Traces 4 to 6: estimated parameters $\mathbf{A}^{est}$, $\mathbf{B}^{est}$, $\mathbf{C}^{est}$ and Traces 7 to 9: estimated parameters misfit A, B and C, respectively.

In AVO analysis, the anomaly detection is usually performed in crossplots between parameters A and B. In this graph, the alignment between A and B in the absence of hydrocarbons defines the expected behavior or the background trend. The Figure 5 shows the crossplots of estimated parameters from the CDP gather. The red points are related to the gas-saturated sandstone and the black ones are related to the oil-saturated sandstone. According

to the classification proposed by Castagna et al. (1998), the gas-saturated sandstone is rated as class 3 anomaly, while the oil-saturated sandstone is rated as class 4. Both anomalies are far from the background trend composed by shales and limestones (green dots.)
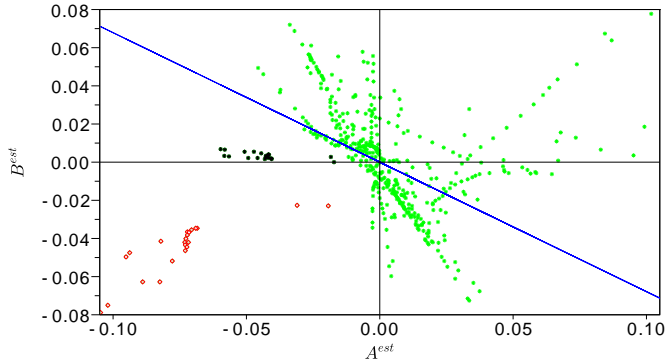

Figure 5: Crossplot between the estimated AVO parameters $\mathbf{A}^{est}$ and $\mathbf{B}^{est}$ (integrated version).

Elastic inversion

Analyzing the amplitude spectrum of the input seismic data, we observe the absence of frequencies below 6 Hz. Figure 6 shows the amplitude spectrum related to the angle-trace for $\theta = 0$. In this case, we applied a trapezoidal band-pass filter defined by 0-0-2-6 Hz on the input logs to create the low-frequency components assumed as a priori information. The amplitude spectrum of these low-frequency components is shown in Figure 7.
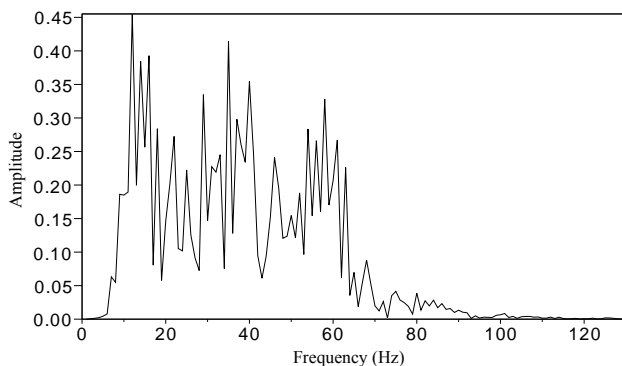

Figure 6: Amplitude spectrum of an angle-trace for $\theta = 0$.

The best fit between the true and estimated parameters was obtained for $\varepsilon = 0.007$ and $\beta = 0.3$, as shown in the Figure 8. I_P was the best estimated parameter whereas ρ presented the worst fit. The results obtained incorporate both high frequency (seismic amplitude information) and the low-frequency trend (well log information).

The Figure 9 shows the parameters estimated when a noisy low-frequency component was considered. To generate this experiment, a low-frequency perturbation was added to v_p. Afterwards, we estimated v_s from v_p using the empirical relation proposed by Castagna et al. (1985)
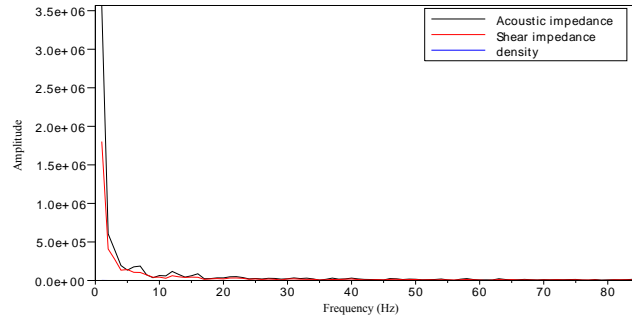

Figure 7: Amplitude spectrum of low-frequency introduced in the elastic inversion.

for mudrocks. The ρ log was estimated from Gardner et al. (1974). This approach is very common in situations where the v_s and ρ controls are inadequate. The fit between the true and estimated I_P is good, but the fit for I_S and ρ is deficient.

It was also simulated a situation where there is a gap for the frequency spectrum from 3 to 6 Hz in the input data. Similar test was done by Lavergne et al. (1979) for acoustic inversion. Figure 10 shows the estimated parameters for this circumstance. Due to the great variation of elastic parameters through reflection time, the generated synthetic CDP gather is very sensitive to the low-frequency content which affects the absolute values estimated of the estimated elastic parameters, mainly for ρ .

A very common technique in the petroleum industry is to analyze the I_P and I_S parameters in crossplots between $I_P - I_S \times I_S$ with the objective to highlight the anomalies related to hydrocarbons and lithologies. From I_P and I_S obtained from well data, we define the cutoff values that characterize the hydrocarbons bearing intervals. The idea is to have in the I_S axis information more related to lithological factors, while in the $I_P - I_S$ axis the information is more related to fluids. Figure 11 shows the crossplots between $I_P - I_S \times I_S$ obtained from well logs. We notice that the gas-saturated (red points) and oil-saturated sandstone (black points) are separated from background trend (green points). Analyzing the values of attributes $I_P - I_S$ and I_S, it is possible to establish the cutoff value for these accumulations. Gas-saturated sandstone: $I_P - I_S < 1150 \ (g/cm^3 \times m/s)$, $I_S < 2100 \ (g/cm^3 \times m/s)$; Oil-saturated sandstones: $I_P - I_S < 2295 \ (g/cm^3 \times m/s)$ and $I_S < 3900 \ (g/cm^3 \times m/s)$.

Figure 12 shows the crossplot between $I_P - I_S \times I_S$ using the result shown in Figure 8. Notice that the inversion procedure did not recovery the adequate absolute values. This fact is attributed to the large elastic contrasts involved in the considered model what causes the approximation given by Fatti et al. (1994) to fail.

The Figure 13 and Figure 14 show the crossplot between elastic parameters estimated for the noisy background and for the low-frequency gap cases, respectively. In Figure 13 the anomalies are not properly characterized while in Figure 14 the absolute values are far from the cutoffs defined in the well data.

It is a common practise to apply a band-pass filter

in the elastic inversion results when the low-frequency components are poorly controlled. Figures 15 and 16 show the result after applying a trapezoidal band-pass filter $(0 - 6 - 70 - 125$ Hz$)$ to crossplots showed in Figures 13 and 14. Notice that the anomaly was recovered after the removal of the low-frequency components, but the absolute values were lost. In this case AVO and elastic inversion results are equivalent.

Conclusion

Both AVO and elastic inversion techniques use information contained in the amplitude variations with offset. The AVO technique is generally qualitative and statistical, while the elastic inversion is more quantitative and deterministic. The tests performed show that in some practical situations a simple AVO analysis is a more robust way of discriminating anomalies related to hydrocarbon-bearing sandstones. The elastic inversion procedure may be very dependent of the knowledge of the low-frequency content. In some situations when the available well control is sparse (i.e exploration phase), it is common to use empirical relationships to estimate shear velocity and density trends from the compressional velocity trend. As shown in this paper, this procedure can produce poor estimates of the elastic parameters. On the other hand, these poor estimates can create and/or distort seismic anomalies. Poor estimated were obtained from the input data containing a gap in the frequency spectrum. In this case the lack of some frequency components prevented a proper recovery of absolute values.

References

Aki, K., and P. G. Richards, 1980, Quantitative seismology: W. H. Freeman and Co.

Castagna, J. P., M. L. Batzle, and Eastwood, 1985, Relationships between compressional-wave and shear-wave velocities in clastic silicate rocks: Geophysics, **50**, 571–581.

Castagna, J. P., H. W. Swan, and D. J. Foster, 1998, Framework for AVO gradient and intercept interpretation: Geophysics, **63**, 948–956.

Fatti, J. L., G. C. Smith, P. J. Vail, P. J. Strauss, and L. P. R., 1994, Detection of gas in sandstone reservoirs using AVO analysis: A 3-D seismic case history using geostack technique: Geophysics, **39**, 770–780.

Gardner, G. H. F., L. W. Gardner, and A. R. Gregory, 1974, Formation velocity and density, the diagnostic basics for stratigraphic traps: Geophysics, **39**, 770–780.

Hampson, D., and B. Russell, 2005, Simultaneous inversion of pre-stack data: SEG Expanded Abstract, **24**, 1633–1637.

Lavergne, M., M. Becquey, and C. Willm, 1979, Acoustic impedance logs computed from seismic traces: Geophysics, **44**, 1485–1501.

Velis, D. R., 2006, Parametric sparse-spike deconvolution and the recovery of the acoustic impedance: SEG Expanded Abstract, **25**, 2141–2145.
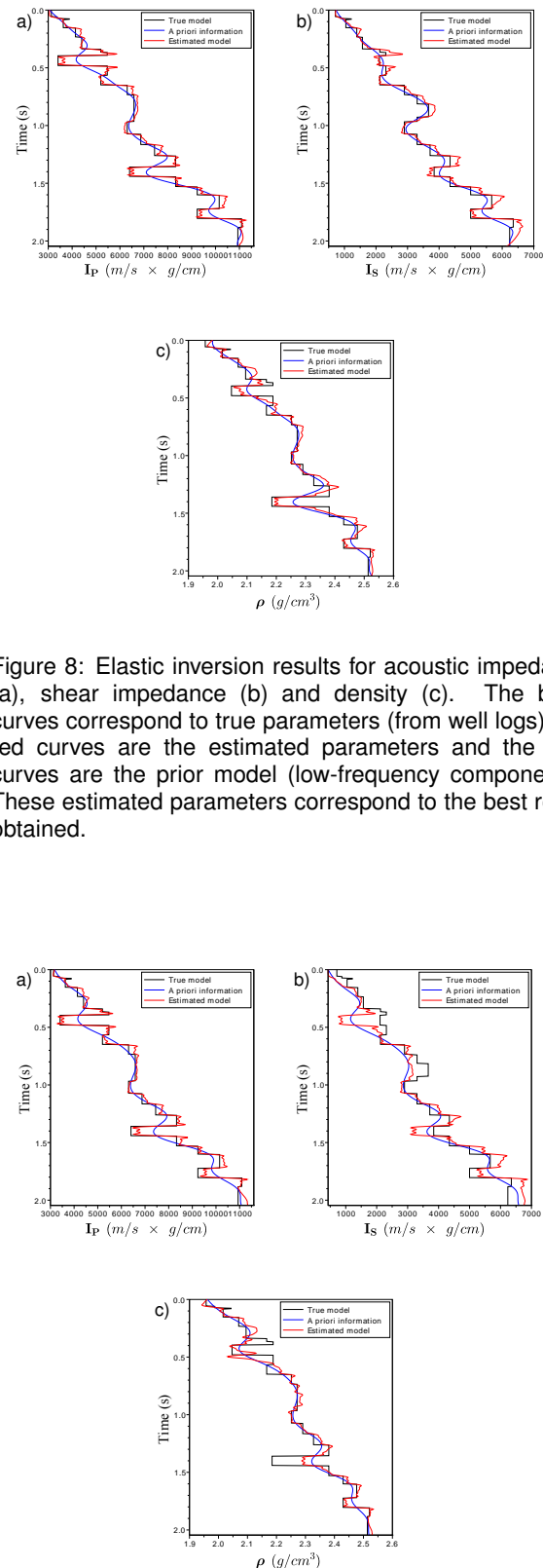
Acknowledgments

Figure 8: Elastic inversion results for acoustic impedance (a), shear impedance (b) and density (c). The black curves correspond to true parameters (from well logs), the red curves are the estimated parameters and the blue curves are the prior model (low-frequency components). These estimated parameters correspond to the best result obtained.

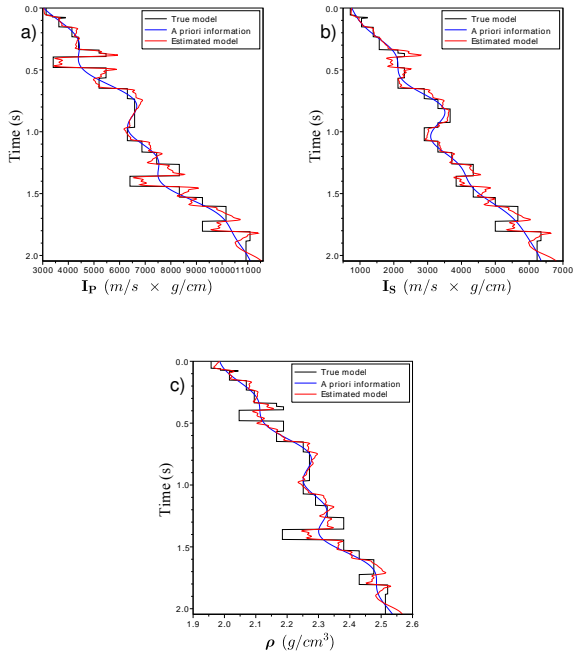Figure 9: Elastic inversion results obtained from a noisy low-frequency components.

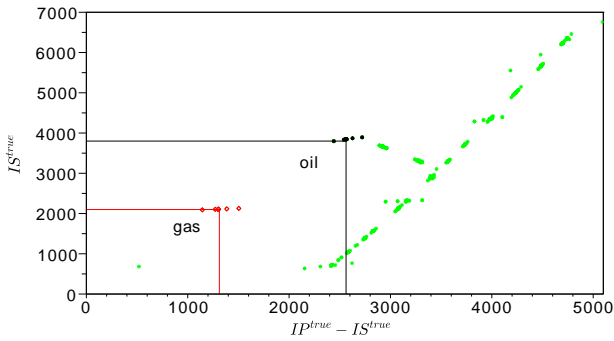Figure 10: Elastic inversion results obtained from a input data with a gap in frequency spectrum.

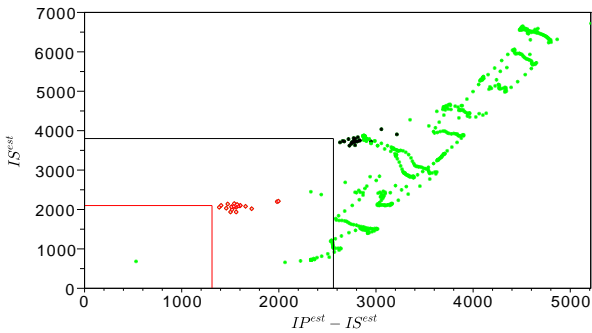Figure 11: Crossplot between the true attributes $I_P - I_S \times I_S$.

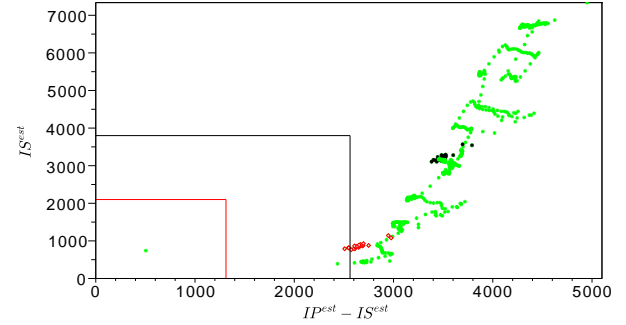Figure 12: Crossplot related to the best estimated parameters.

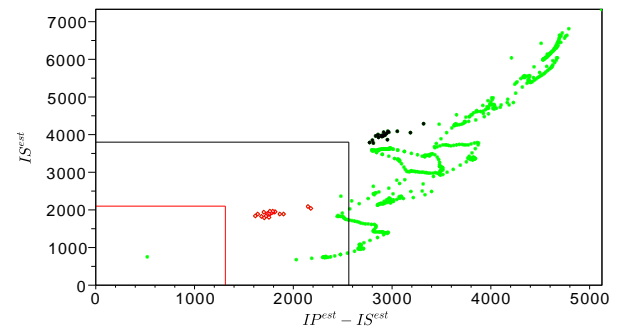Figure 13: Crossplot related to the estimated parameters from a noisy background.

Figure 14: Crossplot related to estimated parameters from the input data containing a gap in frequency spectrum.
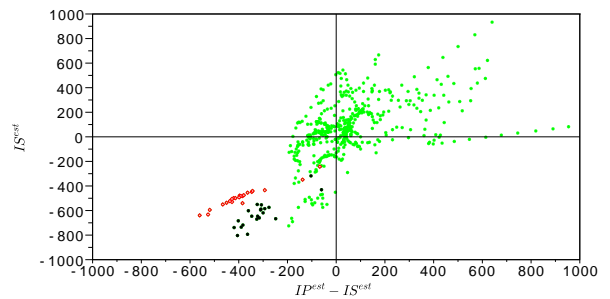

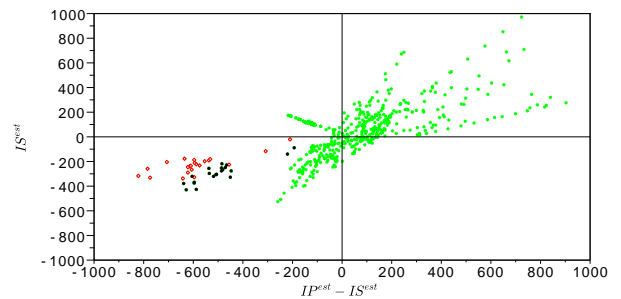Figure 15: Crossplot obtained after the applying of band-pass filter in Figure 13.

Figure 16: Crossplot obtained after the applying of band-pass filter in Figure 14.